

pubs.acs.org/ac Article

# Pattern-Based Recognition Systems: Overcoming the Problem of Mixtures

Michael H. Ihde, Cara F. Pridmore, and Marco Bonizzoni\*



Cite This: Anal. Chem. 2020, 92, 16213-16220



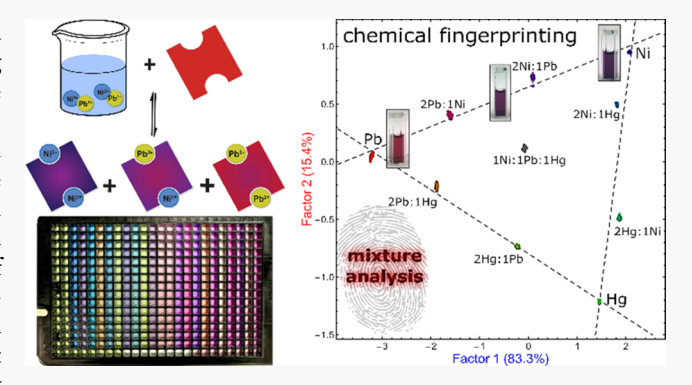
**ACCESS** 

Metrics & More

Article Recommendations

Supporting Information

ABSTRACT: The transformative potential of pattern-based sensing techniques is often hampered by their difficulty in dealing with mixtures of analytes, a drawback that severely limits the applications of this sensing approach (the "problem of mixtures"). We show here that this is not an intrinsic limitation of the pattern sensing method. Indeed, we developed general guidelines for the design of the sensing, signal detection, and data interpretation methods to avoid this constraint, which resulted in chemical fingerprinting systems capable of recognizing unknown mixtures of analytes in a single experiment, without separation or pretreatment before data acquisition. In support of these design principles, we report their successful application to an important analytical problem, metal ion discrimination and quantitation, by



constructing a sensor array that provided a linear colorimetric response over a wide range of analyte concentrations. The resulting data set was interpreted using common multivariate data processing algorithms to achieve quantitative identification and concentration determination for pure and mixture samples, with excellent predictive ability on unknowns. Separation and detection methods for analyte mixtures, normally envisioned as independent processes, were successfully integrated in a single system.

Pattern-based array sensing techniques have gained widespread interest as an analytical tool. In particular, colorimetric and fluorometric sensing arrays have been recognized as an optical analogue to biological sensory systems that allow fast, on-site chemical detection through inexpensive protocols that untrained personnel can carry out on a large number of samples. 1,2 Optical sensing arrays have been studied extensively by our group and others for the detection of a wide variety of analytes including metal ions,<sup>3–7</sup> small organic molecules,<sup>8–18</sup> gases,<sup>19–21</sup> proteins,<sup>22–24</sup> nanoparticles,<sup>25</sup> and bacteria species in biofilm matrices.<sup>26</sup> Moreover, researchers have even used array sensing methods to identify chemical processes, such as molecular aggregation<sup>27</sup> and enzyme activity.<sup>28</sup> Effective cross-reactive arrays are made up of promiscuous receptors, i.e., capable of interacting with multiple (ideally, all) analytes of interest, with significant variations either in the qualitative response or in the observed affinity.<sup>29</sup> They offer a wider scope than the more frequently used selective receptors to detect an assortment of similar analytes that would not be easily distinguished otherwise. By capturing the wealth of information available in the analytes' differential response to the array components, cross-reactive sensing systems often achieve selectivity to lock-and-key-style selective receptors while requiring lower design and synthesis effort and wider scope. 30,31

Despite their significant successes, array sensing systems often fail upon exposure to mixtures of analytes. This can be

typically ascribed to the fact that the analytical response of the underlying chemical sensors is nonlinear, either because they are operating in the nonlinear portion of their response curve or because the chosen signal transduction method responds nonlinearly. Using a scores plot as an example, a common way of presenting results from pattern-based array sensing techniques, this issue is visually summarized in Figure 1. For instance, one can train a pattern detection system to recognize pure substances A and B; one might then assume that the response from a 1:1 mixture of the two would fall halfway between them (a linear response, green section), but that is almost invariably not the case (red section) because of inherent nonlinearities. Therefore, training for the components of a mixture often does not help to recognize the mixture. We refer to this behavior as "the problem of mixtures": sensing arrays are often ineffective at recognizing mixtures, even when they can recognize the individual components.

Researchers have aimed to address this issue, e.g., for mixtures of metal ions, 32-35 proteins, 36-39 and small organic

Received: September 25, 2020 Accepted: November 17, 2020 Published: December 1, 2020





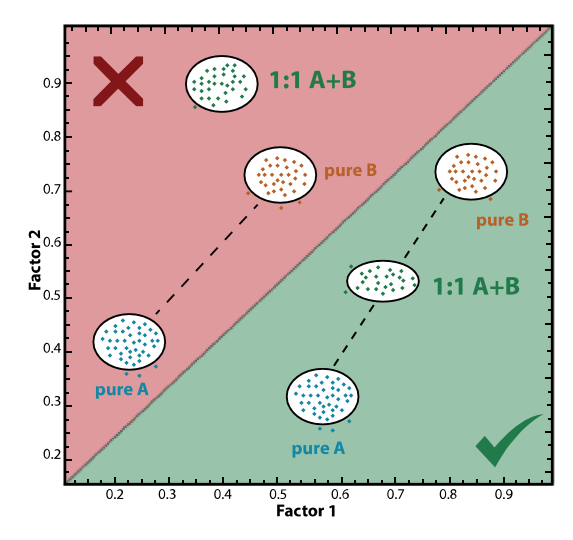


**Figure 1.** Depictions of the linear (green) vs nonlinear (red) relationship between a 1:1 mixture of analytes A and B and the response of its pure components.

molecules, 40-43 employing linear discriminant analysis (LDA), principal component analysis (PCA), or hierarchical cluster analysis (HCA) for data interpretation. While these systems were proficient for their specific endeavors, there has been limited success addressing the source of this problem. Overcoming the "problem of mixtures" for pattern recognition systems will have a profound impact on the detection of multiple similar analytes occurring as mixtures, a recurring problem in analytical science.

In this work, we demonstrate that, by restricting ourselves to using only analytical detection methods that have a rigorously linear response <sup>44,45</sup> and by taking precautions to operate in the regime in which the underlying chemical interactions also respond linearly to changes in concentration, we can then use linear multivariate analytical tools such as LDA and PCA to discriminate mixtures as well as pure analytes. The resulting system would naturally be responsive to changes in analyte concentration in a simple and predictable way, opening a path to the quali-quantitative determination of analytes; calibration plots can be generated to accurately predict the nature and concentration of an unknown mixture of our analytes of choice in a single experiment, without previous separation.

Using metal ion detection as a valuable proof of principle, we introduce here a set of general conditions on the strength of the chemical interaction involved, on the signal transduction method, and on the data interpretation algorithms to ensure that the resulting pattern-based recognition system can identify the composition of analyte mixtures.

#### EXPERIMENTAL SECTION

**Materials.** Xylenol orange (XO) and methylthymol blue (MTB) were purchased from Sigma-Aldrich and used as received. 2-[4-(2-Hydroxyethyl)piperazin-1-yl]ethanesulfonic acid (HEPES) was purchased from ICI Scientific. All metal chloride salts were bought from Fluka. For consistency, all stock solutions for dyes and metal chloride salts were prepared fresh before each experiment. All experiments were carried out in a 50 mM HEPES aqueous solution buffered to pH 7.4, prepared by adding an appropriate amount of HEPES free acid to deionized (DI) water; the pH was then adjusted to 7.4 by adding 1.0 M NaOH as needed, monitoring with a combined

glass electrode, and then bringing up to volume. Stock solutions of XO and MTB were prepared in this buffer, taking into consideration the manufacturer specified dye content (90% and 70% for XO and MTB, respectively). All metal chloride salt stock solutions (except PbCl<sub>2</sub>) were prepared by adding an appropriate amount of salt to 10 mL of buffer. Lead(II) chloride solutions were prepared by dissolving a minimal amount of salt in DI water and diluting an appropriate aliquot of this solution in buffer. To avoid unwanted absorption of water over time, any hygroscopic salts (ZnCl<sub>2</sub>, CdCl<sub>2</sub>, MgCl<sub>2</sub>, and BaCl<sub>2</sub>) were dried to constant weight in an oven set to 110 °C and stored in a desiccator before use.

**Instrumentation.** Benchtop UV—vis measurements were performed on a Hewlett-Packard 8452A diode array UV—vis spectrophotometer. The experimental sample temperature was thermostatted to 25 °C using an external circulating water bath. Multivariate data was acquired on a BioTek Synergy II microwell plate reader equipped with a monochromator to measure absorbance spectra. The sample compartment was electrically thermostatted. Experiments were laid out by hand using Eppendorf Research multichannel pipettors and disposable plastic tips into Greiner BioOne nontreated polystyrene 384-well microplates with clear flat bottoms. Each well was filled with  $100~\mu\text{L}$  of solution. Plates were read immediately after preparation. Reading time was 10-15 min per plate during which no evaporation was observed so the plates were not sealed.

## ■ RESULTS AND DISCUSSION

Design of Sensing Array for Mixtures. We chose UV—vis absorbance spectroscopy for analytical signal transduction due to the linear dependence of signal intensity (absorbance) on concentration when conditions are chosen appropriately. We also chose the detection of divalent metal cations and their mixtures as a testbed for our design principles. Since these analytes can form stable complexes with many well-known, readily available dyes, complex formation is nearly quantitative under practically relevant conditions, and the corresponding change in the dye's electronic absorption is linear over a wide range of metal concentrations.

Sifting through the literature on colorimetric metal ion determination provided several metal-binding dye candidates. Our screening results, shown in Figure S1 in the Supporting Information, found two excellent candidates for inclusion in a cross-reactive array, xylenol orange (XO) and methylthymol blue (MTB), which are shown in Figure 2. The sodium salts of these anionic dyes are remarkably water-soluble and commercially available in adequate purity, and they have long been known to form strong coordination complexes with a multitude of metal ions. 46,47

Figure 2. Chemical structures of xylenol orange (XO) and methylthymol blue (MTB) in their protonation state in neutral water solution (pH = 7.4).

To ascertain their cross-reactive behavior and linear response, we conducted titrations of each dye with aliquots of metal(II) chloride in neutral water. As metal cations were added, the absorption spectrum varied depending on both the concentration and nature of the metal. The cross-reactive, differential responses of both dyes to several divalent metal ions are shown in Figure 3.

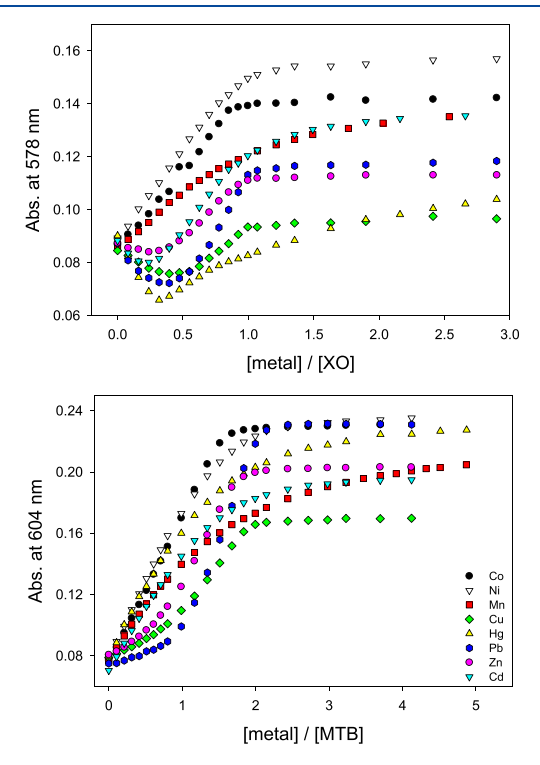


**Figure 3.** Isotherms from the titration of aliquots of eight metal(II) chlorides into solutions of xylenol orange (XO, 5.0  $\mu$ M, top) and methylthymol blue (MTB, 7.5  $\mu$ M, bottom) in buffered water (pH 7.4, 50 mM HEPES).

With increasing metal ion concentration, clear differences in behavior were observed. For example, at an M(II)/XO ratio of 2:1, very marked differences in the absorbance of the XO/metal complex were apparent at 578 nm; comparison of  $\rm Zn^{II}$  vs  $\rm Cu^{II}$  vs  $\rm Ni^{II}$  also shows remarkable variability. This varied behavior reflects the underlying differences in binding modes (e.g., geometry and stoichiometry) for those metal ions. On the other hand, both dyes were much less responsive to s-block divalent metal cations (see Figure S11) and to Na<sup>+</sup>. Since Na<sup>+</sup> is a ubiquitous interferent in the determination of other metal ions in any matrix of practical relevance, insensitivity to Na<sup>+</sup> is actually welcome for the current application.

Working at relatively low dye concentrations ([dye] = 5 and 7.5  $\mu$ M for XO and MTB, respectively), formation constants for the metal—dye complexes could be determined for most metal cations with XO and MTB dyes from absorption profiles such as those presented in Figure 3 (see Table S1and Figure S4 in the Supporting Information). The 1:1 formation constants for the dye/metal complexes ranged from  $10^5$  to  $10^{10}$ , indicating wide variability in binding affinity and yet strong binding throughout.

In addition to those observed at 578 nm (for XO) and 604 nm (for MTB) in Figure 3, further differences were also evident in other parts of the absorption spectrum of each

metal-dye complex (see Figures S2 and S3 in the Supporting Information). Taken together, such features may allow one to identify the metal to which the dye is responding by careful comparison of the absorbance spectra at a relatively high concentration of metal. However, distinguishing metals at lower concentrations would become increasingly difficult: instead, the spectroscopic information was interpreted using pattern recognition-based methods. The varied response to the metal ions under test, the high signal intensity, and the excellent dynamic range make these dyes compelling promiscuous chemical sensors. The strength of these complexes allowed us to find conditions for the analytical response to be linear with the mixture's composition. Indeed, all isotherms shown in Figure 3 display a distinct linear region at low metal concentration where the spectral response varies linearly with the concentration of metal cation, providing an ideal testbed for our design hypothesis.

Metal Ion Discrimination. For repeatable acquisition of absorption data at multiple wavelengths on many analytes, samples were laid out on 384-well microplates and experiments were conducted on an automated plate reader. Plates contained enough space for multiple replicates of each metal sample, together with dye reference standards and buffer blanks. For our initial qualitative experiment, the sensing array was exposed to 11 divalent metal chloride salts: Ba<sup>II</sup>, Mg<sup>II</sup>, Fe<sup>II</sup>, Mn<sup>II</sup>, Co<sup>II</sup>, Ni<sup>II</sup>, Cu<sup>II</sup>, Hg<sup>II</sup>, Cd<sup>II</sup>, Zn<sup>II</sup>, and Pb<sup>II</sup>; each salt was dissolved in H<sub>2</sub>O containing 50 mM HEPES buffer (2-[4-(2hydroxyethyl)piperazin-1-yl]ethanesulfonic acid) adjusted to pH 7.4. Biasing effects stemming from the metals' counterion were avoided by using chloride salts throughout since Cl<sup>-</sup> is a well-solvated, relatively inert anion in neutral water. 48 Sodium chloride was also added to the analyte panel as a negative control since neither dye was expected to respond to it according to the preliminary work described above. Furthermore, selected transition metal complexes from our panel are susceptible to pH-dependent hydrolysis, so the pH of all solutions was carefully controlled. For instance, Fe<sup>II</sup> may be oxidized to Fe<sup>III</sup> by dissolved oxygen in water;<sup>49</sup> the resulting acidic Fe<sup>III</sup> aqua complex can then hydrolyze to form insoluble precipitates, leading to inconsistent metal concentration. Therefore, all stock solutions were prepared fresh before each experiment and were kept at constant pH and temperature.

For all qualitative experiments, absorbance was monitored at 334, 342, 360, 380, 400, 436, 442, 450, 482, 500, 520, 540, 560, 578, 590, 604, and 614 nm, the positions of prominent features in the absorbance spectra of the metal complexes of XO and MTB found during binding titrations (see Figure S6 in the Supporting Information). For differentiation work, metal concentrations were kept constant at 5  $\mu$ M and dye concentrations were set to the same used in the benchtop binding titrations mentioned previously, namely, 5  $\mu$ M and 7.5 μM for XO and MTB, respectively. Fifteen replicates were prepared for each metal sample, which generated a large data set (2 dyes  $\times$  12 analytes  $\times$  15 replicates = 360 samples, each described by the 17 measured absorbance values listed above). A detailed layout of the microwell plate containing these solutions and a picture of the completed plate that showcases the highly differential colorimetric response are shown in Figure S5.

Linear discriminant analysis (LDA) was then used to aid in data analysis and dimensionality reduction. The LDA algorithm generates a new data set whose descriptor variables are linear combinations of the original instrumental measure-

ments, constructed so that maximum separation between samples is achieved while at the same time minimizing separation between replicate measurements for the same analyte to give tight, well-separated clusters.<sup>51</sup> These descriptors, called factors, are returned in decreasing order of information content, allowing for straightforward dimensionality reduction: one can drastically reduce the size of the data set by retaining only the first few important factors, with minimal loss of information. We chose to retain two factors, so each sample in the transformed data set was associated with a pair of numbers, its factor scores, which could be used as coordinates to plot the transformed data points in a twodimensional graph, the scores plot. The factor loadings obtained from the LDA analysis, i.e., the contributions of each measurement to the LDA factors, indicate that some of them contributed very little to the performance of the array in separating metal ions. These superfluous instrumental measurements introduce noise and require extra acquisition time so, in a process referred to as "variable reduction", we optimized the sensing system by removing instrumental measurements from the original data set. The details of the "variable reduction" process for the  $[M^{II}] = 5 \mu M$  qualitative data set are described further in the Supporting Information (Figure S8).

The plots of LDA scores and loadings for the qualitative discrimination of divalent metal cations, obtained after variable reduction, are presented in Figure S9 in the Supporting Information. The tight clustering and good separation in the scores plot indicate excellent repeatability and strong discriminatory power, respectively; in short, they show that this cross-reactive sensor array was very effective in discriminating all metal cations of analytical interest. Furthermore, analysis of the loadings plot (Figure S9) showed that the two dyes are both contributing meaningfully to the differentiation, indeed in almost equal proportions, an ideal situation for pattern-based sensing procedures. Further details on the qualitative results can be found in the Supporting Information. Having shown that the system responds linearly to changes in concentration of metal ions, we moved to qualiquantitative analytical determinations.

Quantitative Analysis. Quantitative work would hinge critically on retaining a linear response from the dye/metal complex formation system. However, Figure 3 above shows that the system responds linearly only over a specific range of metal concentrations. In pursuing quantitative response, therefore, we redesigned the array to include multiple solutions of each dye, each at a different concentration: this guaranteed that, for any practically relevant concentration of metal ions, one of these dye solutions would exhibit the sought after linear response to the metal concentration, and the others would "fall silent", having no significant response: they would be either too concentrated and therefore give off a constant, high saturated signal or too dilute and insensitive, giving off a constant, low signal. The LDA analysis would then automatically discard these contributions from the out-of-range dye solutions due to their low variance, i.e., no information content useful for sample discrimination.

We selected four divalent metal ions to run our test (Cd<sup>II</sup>, Hg<sup>II</sup>, Pb<sup>II</sup>, and Cu<sup>II</sup>) for their biological and environmental importance. On a 384-well microplate, our sensing array comprised three concentrations for each dye (5, 20, and 40  $\mu$ M for XO and 10, 30, and 60  $\mu$ M for MTB). We laid out a series of samples at five concentrations for each metal cation (1, 2.5,

5, 7.5, and 10  $\mu$ M). Using LDA analysis and the reduced variable set obtained previously, the array was able to differentiate all concentrations of these metal ions with clear linear characteristics. In this case, 54 total instrumental measurements for each dye concentration were reduced to 18 (see Figure S14 for the loadings plot). The resulting LDA scores plot (Figure 4) displays excellent separation between clusters of replicates.

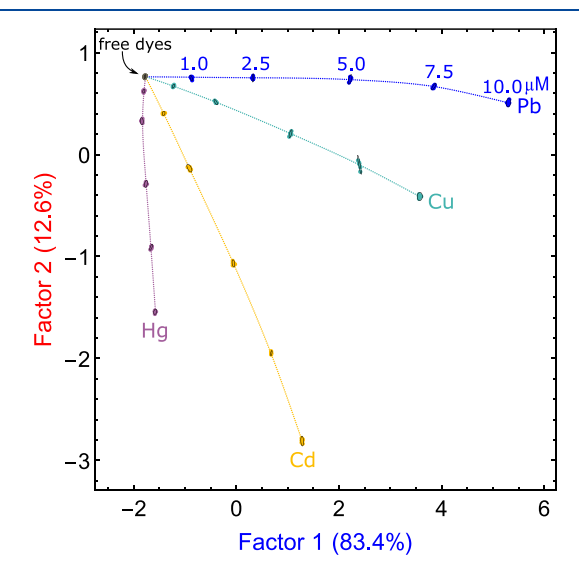


**Figure 4.** LDA scores plot for the quali-quantitative differentiation of  $Cd^{II}$ ,  $Hg^{II}$ ,  $Pb^{II}$ , and  $Cu^{II}$  at five concentrations (1, 2.5, 5, 7.5, and 10  $\mu$ M; [XO] = 5, 20, and 40  $\mu$ M and [MTB] = 10, 30, and 60  $\mu$ M).

These results clearly show that the system is capable of quantitative and qualitative differentiation of these metal cations: in other words, if one were to process an unknown in the same way as these training samples, the unknown's position on the plot would not only indicate which metal was present but also at what concentration. This is a remarkable result for such a simple system at relatively low concentration in neutral water.

Analysis of Mixtures. The remarkably good discriminatory power coupled with linearity in concentration response obtained above provided the necessary foundation to confront the "problem of mixtures" to which we referred before. We therefore challenged the array with a series of mixtures of metal cations, intending to use its response as a 2D calibration curve.

In the following work, we examined binary and ternary mixtures of NiCl<sub>2</sub>, HgCl<sub>2</sub>, and PbCl<sub>2</sub>. On a 384-well microplate, three solutions containing pure metal ions (30  $\mu$ M), one equimolar ternary mixture (10  $\mu$ M each), and six stock solutions containing 2:1 binary mixture combinations of each metal ([metal] =20 and 10  $\mu$ M) were added to the array. Higher dye concentrations offered better overall signal-to-noise ratios in this case ([MTB] = 30  $\mu$ M, [XO] = 20  $\mu$ M; see the Supporting Information for comparison). After LDA analysis, dimensionality reduction, and retention of the nine most important instrumental measurements (out of the 24 collected), the resulting LDA scores plot, which retained 98.7% of the original information, is shown in Figure 5.

Encouragingly, the three pure metals and mixture samples were found distributed along the edges of a triangle, with the pure metal samples at each vertex. For each pair of metal ions, the corresponding 1:2 and 2:1 mixtures were found where

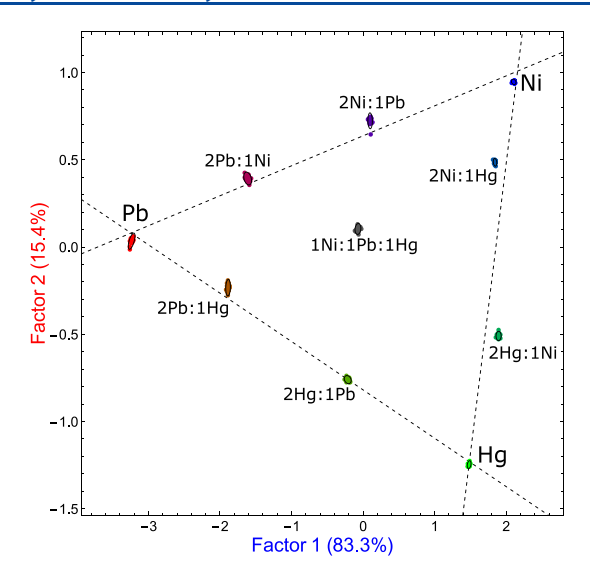


**Figure 5.** Two-dimensional LDA scores plot for the separation of metal ion mixtures. The plot was obtained using only the nine most important instrumental measurements and captures 98.7% of the total information content from the original data set ([XO] = 20  $\mu$ M and [MTB] = 30  $\mu$ M, total [M<sup>II</sup>] = 30  $\mu$ M).

expected, namely, one third and two thirds of the way along the triangle's corresponding edge, respectively. Furthermore, replicates from the equimolar ternary mixture clustered very close to the center of the triangle identified by the pure metal clusters. To highlight the quality of the positional response, we calculated best-fit trendlines for each of the triangle's sides; for instance, the trendline on the top left of Figure 5 was obtained by drawing a best-fit line through the centroids of the clusters for Pb<sup>II</sup>, 2Pb<sup>II</sup>:Ni<sup>II</sup>, Pb<sup>II</sup>:2Ni<sup>II</sup>, and Ni<sup>II</sup>. The replicate clusters also remained very tight (excellent reproducibility) and widely spaced (high discriminatory power).

To further support the generality of this approach, the same array was exposed to metal ion mixtures composed of three different metal cations. Thus, the same binary and ternary mixtures used previously for Ni<sup>II</sup>, Pb<sup>II</sup>, and Hg<sup>II</sup> were prepared using CoCl2, CuCl2, and CdCl2 and added to a 384-well microplate under the conditions described previously. After LDA analysis, dimensionality reduction, and retention of the eight most important variables, a two-dimensional plot of LDA scores was generated, shown in Figure 6. These results appear nearly identical to those shown previously for Ni<sup>II</sup>, Pb<sup>II</sup>, and Hg<sup>II</sup> (Figure 5): the three pure metal clusters make up the vertices of a triangle, the 2:1 binary mixtures are distributed appropriately along its edges, and the equimolar ternary mixture replicates are positioned near the center of the triangle. Once again, all replicate clusters display tight intra-cluster spacing (indicating high reproducibility), with large intercluster distances (high discriminatory power). These results, obtained using a second set of metal cations, confirm that our previous success was not due to the specific analytes chosen but due to the choice of conditions, which should therefore allow for discrimination of any mixture of metal cations, as long as they display appreciable affinity toward these dyes. Because most transition and heavy metals do, this bodes well for the generality of this method.

Identification of Binary Mixtures of Unknown Composition. Knowing that the system responds linearly to variations in relative composition of these mixtures, we used

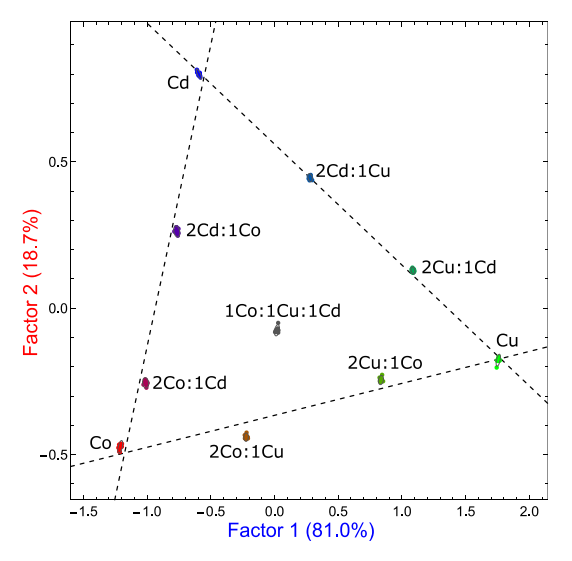


**Figure 6.** Two-dimensional LDA scores plot for the separation of a metal ion mixtures ( $Co^{II}$ ,  $Cu^{II}$ , and  $Cd^{II}$ ). The plot was obtained using the eight most important instrumental measurements and captures 99.7% of the total information content from the original data set ( $[XO] = 20 \ \mu M$  and  $[MTB] = 30 \ \mu M$ , total  $[M^{II}] = 30 \ \mu M$ ).

the results in Figure 5 as a training set to identify mixtures of unknown composition, some among which were not included in the original training set (e.g., 1:1 binary mixtures). We asked a colleague to prepare eight metal ion solutions whose composition was unknown to us and exposed the array to each of them under the same conditions as the training set. The measurements obtained from this test set were transformed using the LDA eigenvectors (transformation rules) generated from the training set. As a result, the test set data could be projected onto the training set scores plot from Figure 5. The results, displayed in Figure 7, accurately predict the composition of unknown samples in the challenge set.

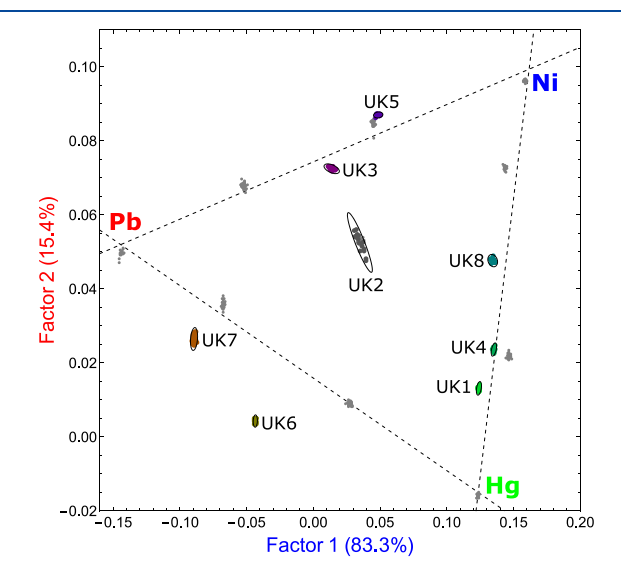


**Figure 7.** LDA scores plot for the test set of eight unknown metal ion mixtures (UK*n*) onto the training set from Figure 5, generated using the same conditions. 98.7% of the information content in the raw set was retained. UK1: 5:1 Hg/Ni, UK2: 1:1:1 Ni/Pb/Hg, UK3: 1:1 Ni/Pb, UK4: 2:1 Hg/Ni, UK5: 2:1 Ni/Pb, UK6: 1:1 Pb/Hg, UK7: 2:1 Pb/Hg, and UK8: 1:1 Ni/Hg.

Included in the challenge set was also an equimolar ternary mixture, found to overlap with the same cluster from the training set. Additionally, all binary mixtures from the challenge set were found in the predicted positions along the trend lines obtained from the training set. Notably, this included four binary mixtures that had not been present in the training data (three 1:1 binary mixtures and a 5:1  ${\rm Hg^{II}/Ni^{II}}$ ), and yet the system was able to place them in appropriate positions on the calibration plot. Thus, enforcement of a strictly linear behavior provided a predictable response capable of identifying features for which the system had not been trained

#### Identification of Ternary and Quaternary Mixtures.

We then attempted to identify four unequal ternary mixtures of the same three metal cations; none of these mixtures was present in the training set. We prepared three solutions containing 20  $\mu$ M of one metal and 5  $\mu$ M of the other two as well as a 3:2:1 mixture, containing 15  $\mu$ M Ni<sup>II</sup>, 10  $\mu$ M Pb<sup>II</sup>, and 5  $\mu$ M Hg<sup>II</sup>. After taking the same nine instrumental measurements as the training set, Figure 8 shows the results

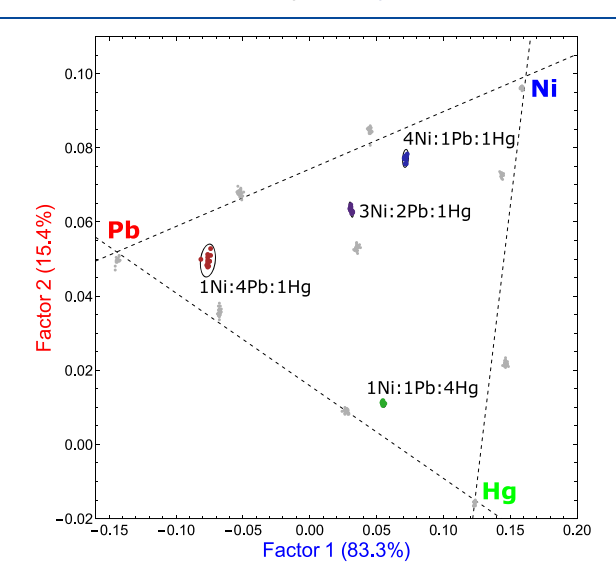


**Figure 8.** Two-dimensional plot of the LDA scores for the "ternary test set", projecting four unequal ternary metal ion mixtures onto the training set from Figure 5 ([XO] = 20  $\mu$ M and [MTB] = 30  $\mu$ M, total [M<sup>II</sup>] = 30  $\mu$ M).

obtained when this ternary challenge set was projected onto the training set previously shown in Figure 5. As expected, all ternary mixtures fall inside the triangle delineated in the training set. The array's ability to distinguish the most abundant metal ion in the 4:1:1 mixtures was particularly impressive. Moreover, the position of the 3:2:1 ternary mixture cluster is correctly placed relative to the equimolar ternary mixture cluster from the training set. In short, the system was very successful in identifying the relative composition of four ternary mixtures that had not been included in the initial training set.

Pushing further, the same sensing array ([XO] =  $20 \mu M$ , [MTB] =  $30 \mu M$ ) was then exposed to a series of mixtures composed of four metal chlorides (total [M<sup>II</sup>] =  $36 \mu M$ , CuCl<sub>2</sub>, PbCl<sub>2</sub>, HgCl<sub>2</sub>, and CdCl<sub>2</sub>). For this study, the analyte panel included an equimolar quaternary mixture, all 12 possible 2:1 binary mixtures, and the four pure metal samples. In this case, three factor scores were retained for each sample resulting in

the 3D plot displayed in Figure 9, in which the equimolar quaternary mixture was positioned at the center of a

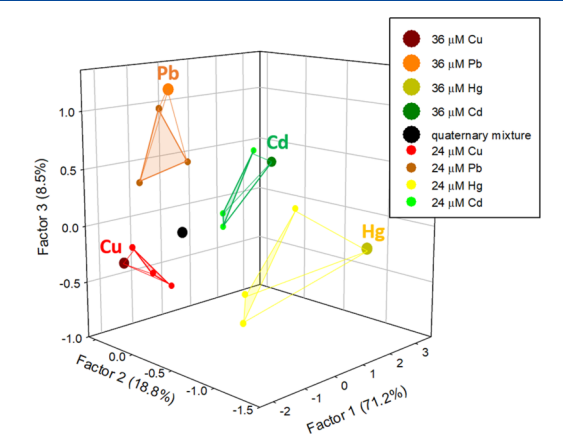


**Figure 9.** Discrimination of quaternary mixtures of metal ions by LDA. For clarity, 2:1 binary mixtures are not explicitly labeled and only cluster centroids are shown ([XO] = 20  $\mu$ M, [MTB] = 30  $\mu$ M, total [M<sup>II</sup>] = 36  $\mu$ M in H<sub>2</sub>O solution buffered to pH 7.4 with 50 mM HEPES).

tetrahedron whose vertices correspond to the four pure metal samples. Moreover, the most abundant metal in each 2:1 binary mixture combination was positioned nearest to the respective pure metal vertex, between the pure metal and equimolar mixture points within the confines of the tetrahedron. These results further highlight that carefully ensuring a linear response translated in the system's predictable behavior when exposed to mixtures of analytes.

Response to Total Metal Ion Concentration. Finally, we examined the array's response to variations of total metal concentrations. Up to this point, all mixtures contained a total metal ion concentration of 30  $\mu$ M. Using the same array setup, we explored how the response changed as a function of total metal concentration. We acquired a second training set at a lower total [metal ion], namely, 15  $\mu$ M. Assuming that the response of the array scales linearly with total metal concentration, one would then be able to determine the nature and concentration of the metal ions under study and their mixtures in a single experiment.

We repeated the procedure used to generate the training set for mixture analysis but with total metal ion concentration cut in half to 15  $\mu$ M. The 2D scores plot obtained for metal ion mixtures at 15  $\mu$ M was comparable to the one obtained for the 30  $\mu$ M systems shown in Figure 5 and Figure 6 (see Figure S16 in the Supporting Information).

Combining the 30  $\mu$ M and 15  $\mu$ M data sets generated a 3D scores plot displaying very clear separation of the two concentration data sets (Figure 10). The data set corresponding to each concentration retained a roughly triangular shape; within each triangle, whose vertices corresponded to the pure metal samples, mixtures were positioned at the appropriate intermediate positions along each edge. Furthermore, the two triangular ensembles corresponding to the two total metal concentration values stacked up well in 3D "factor space", highlighting the relationship between the two data sets.

Connecting the vertices of the triangles obtained from each metal ion concentration for the same metal ion also allowed us to extrapolate the array's behavior at infinite sample dilution (i.e.  $[M^{II}] \approx 0~\mu M$ ). We found that the extrapolated behavior

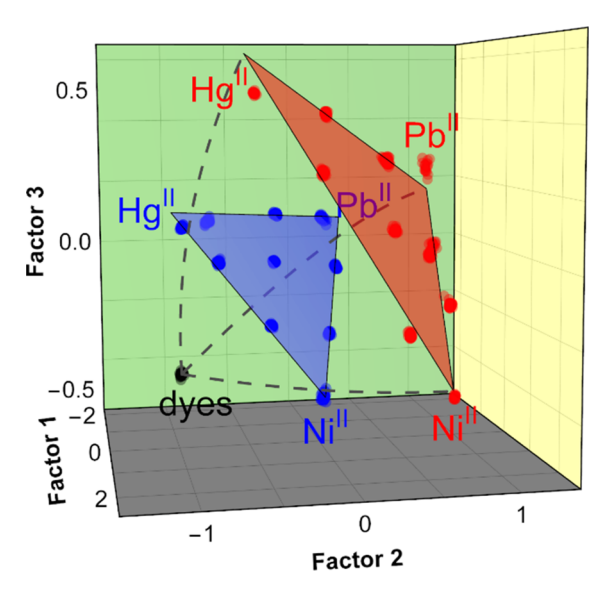


**Figure 10.** Three-dimensional LDA scores plot of the combined 15  $\mu$ M (blue) and 30  $\mu$ M (red) data sets. Dotted lines connecting corresponding pure metal sample clusters extend to the no-metal cluster at [M<sup>II</sup>] = 0  $\mu$ M (labeled "dyes" in the plot).

matched well with the one observed experimentally for samples containing the dyes alone (i.e.  $[M^{II}] = 0~\mu M$ , black dots in Figure 9), further confirming that the sensor array's response scales linearly with the concentration of the metal analytes. This is an important result that demonstrates the array's ability to determine the concentration of these analytes, in addition to their identity: the array can determine the identity and concentration of a sample containing any mixture of Ni<sup>II</sup>, Pb<sup>II</sup>, and Hg<sup>II</sup> over a range of concentrations between 0 and 30  $\mu$ M. In fact, it should be possible to extend the effective concentration range, if all components of the analytical system respond linearly.

## CONCLUSIONS

We developed a cross-reactive, multivariate sensing array consisting of two well-known, commercially available dyes that were selected to form strong coordination complexes with a variety of divalent metal cations in neutral buffered water. On this simple basis, we constructed a robust approach for direct quantitative multivariate sensing of analytes in a mixture based on specific criteria for the detection of analytically relevant metal ion targets, removing the need for chemical separation prior to detection. The design principles presented in this paper are general and can be applied to other array-based systems: once response linearity is achieved, the results can be used as effective and simple multidimensional "calibration plots" to identify the makeup of analyte mixtures of unknown composition. Separation and detection methods for analyte mixtures, normally envisioned as independent processes, were integrated in a single system.

## ASSOCIATED CONTENT

## Supporting Information

The Supporting Information is available free of charge at https://pubs.acs.org/doi/10.1021/acs.analchem.0c04062.

Additional UV-vis titration spectra, pH titrations, binding constant determination, further experimental details for multivariate analysis (data processing

procedures, variable reduction, and PCA results), and determination of limit of differentiation (PDF)

#### AUTHOR INFORMATION

## **Corresponding Author**

Marco Bonizzoni — Department of Chemistry and Biochemistry, The University of Alabama, Tuscaloosa, Alabama 35487-0336, United States; Alabama Water Institute, Tuscaloosa, Alabama 35487, United States; orcid.org/0000-0003-0155-5481;

Email: marco.bonizzoni@ua.edu

#### **Authors**

Michael H. Ihde – Department of Chemistry and Biochemistry, The University of Alabama, Tuscaloosa, Alabama 35487-0336, United States

Cara F. Pridmore – Department of Chemistry and Biochemistry, The University of Alabama, Tuscaloosa, Alabama 35487-0336, United States

Complete contact information is available at: https://pubs.acs.org/10.1021/acs.analchem.0c04062

#### **Funding**

This work was funded by the National Science Foundation (OIA 1632825).

#### **Notes**

The authors declare no competing financial interest.

#### ACKNOWLEDGMENTS

We gratefully acknowledge the financial support from The University of Alabama and the National Science Foundation. We also acknowledge support from the Alabama Water Institute and David Galinat's help for fruitful discussion on the graphical presentation of results.

## ABBREVIATIONS

HEPES 2-[4-(2-hydroxyethyl)piperazin-1-yl]ethanesulfonic acid

LDA linear discriminant analysis

MTB methylthymol blue

PCA principal component analysis

XO xylenol orange

## REFERENCES

- (1) Li, Z.; Askim, J. R.; Suslick, K. S. Chem. Rev. 2019, 119, 231–292.
- (2) Sarkar, T.; Selvakumar, K.; Motiei, L.; Margulies, D. Nat. Commun. 2016, 7, 11374.
- (3) Sasaki, Y.; Minamiki, T.; Tokito, S.; Minami, T. Chem. Commun. 2017, 53, 6561-6564.
- (4) Mallet, A. M.; Davis, A. B.; Davis, D. R.; Panella, J.; Wallace, K. J.; Bonizzoni, M. Chem. Commun. **2015**, *51*, 16948–16951.
- (5) Xu, W.; Ren, C.; Teoh, C. L.; Peng, J.; Gadre, S. H.; Rhee, H.-W.; Lee, C.-L. K.; Chang, Y.-T. *Anal. Chem.* **2014**, *86*, 8763–8769.
- (6) Wang, Z.; Palacios, M. A.; Anzenbacher, P., Jr. Anal. Chem. 2008, 80, 7451–7459.
- (7) Lee, J. W.; Lee, J.-S.; Kang, M.; Su, A. I.; Chang, Y.-T. Chem. Eur. J. 2006, 12, 5691–5696.
- (8) Tropp, J.; Ihde, M. H.; Williams, A. K.; White, N. J.; Eedugurala, N.; Bell, N. C.; Azoulay, J. D.; Bonizzoni, M. Chem. Sci. 2019, 10, 10247–10255.
- (9) Pushina, M.; Farshbaf, S.; Shcherbakova, E. G.; Anzenbacher, P., Jr. Chem. Commun. **2019**, 55, 4495–4498.

- (10) Wang, B.; Han, J.; Bojanowski, N. M.; Bender, M.; Ma, C.; Seehafer, K.; Herrmann, A.; Bunz, U. H. F. *ACS Sens.* **2018**, *3*, 1562–1568
- (11) Huang, W.; Bender, M.; Seehafer, K.; Wacker, I.; Schröder, R. R.; Bunz, U. H. F. Macromolecules 2018, 51, 1345-1350.
- (12) Liang, X.; Bonizzoni, M. J. Mater. Chem. B 2016, 4, 3094–3103.
- (13) Askim, J. R.; Li, Z.; LaGasse, M. K.; Rankin, J. M.; Suslick, K. S. Chem. Sci. **2016**, 7, 199–206.
- (14) Minami, T.; Esipenko, N. A.; Zhang, B.; Isaacs, L.; Anzenbacher, P., Jr. Chem. Commun. **2014**, 50, 61–63.
- (15) Mallet, A. M.; Liu, Y.; Bonizzoni, M. Chem. Commun. 2014, 50, 5003–5006.
- (16) Liu, Y.; Bonizzoni, M. J. Am. Chem. Soc. 2014, 136, 14223–14229.
- (17) Lin, H.; Jang, M.; Suslick, K. S. J. Am. Chem. Soc. 2011, 133, 16786–16789.
- (18) Zhang, C.; Suslick, K. S. J. Am. Chem. Soc. 2005, 127, 11548-11549.
- (19) Joy, N. A.; Rogers, P. H.; Nandasiri, M. I.; Thevuthasan, S.; Carpenter, M. A. Anal. Chem. 2012, 84, 10437–10444.
- (20) Rakow, N. A.; Suslick, K. S. Nature 2000, 406, 710-713.
- (21) Li, Z.; Suslick, K. S. Anal. Chem. 2019, 91, 797-802.
- (22) Pode, Z.; Peri-Naor, R.; Georgeson, J. M.; Ilani, T.; Kiss, V.; Unger, T.; Markus, B.; Barr, H. M.; Motiei, L.; Margulies, D. Nat. Nanotechnol. 2017, 12, 1161–1168.
- (23) Sun, W.; Lu, Y.; Mao, J.; Chang, N.; Yang, J.; Liu, Y. Anal. Chem. 2015, 87, 3354–3359.
- (24) Xu, S.; Lu, X.; Yao, C.; Huang, F.; Jiang, H.; Hua, W.; Na, N.; Liu, H.; Ouyang, J. Anal. Chem. **2014**, 86, 11634–11639.
- (25) Mahmoudi, M.; Lohse, S. E.; Murphy, C. J.; Suslick, K. S. ACS Sens. **2016**, *1*, 17–21.
- (26) Ngernpimai, S.; Geng, Y.; Makabenta, J. M.; Landis, R. F.; Keshri, P.; Gupta, A.; Li, C.-H.; Chompoosor, A.; Rotello, V. M. ACS Appl. Mater. Interfaces 2019, 11, 11202–11208.
- (27) Hatai, J.; Motiei, L.; Margulies, D. J. Am. Chem. Soc. 2017, 139, 2136–2139.
- (28) Zamora-Olivares, D.; Kaoud, T. S.; Zeng, L.; Pridgen, J. R.; Zhuang, D. L.; Ekpo, Y. E.; Nye, J. R.; Telles, M.; Anslyn, E. V.; Dalby, K. N. ACS Chem. Biol. 2020, 15, 83–92.
- (29) Kitamura, M.; Shabbir, S. H.; Anslyn, E. V. J. Org. Chem. 2009, 74, 4479–4489.
- (30) You, L.; Zha, D.; Anslyn, E. V. Chem. Rev. 2015, 115, 7840-7892.
- (31) Geng, Y.; Peveler, W. J.; Rotello, V. M. Angew. Chem., Int. Ed. **2019**, 58, 5190–5200.
- (32) Feng, C.; Zhao, P.; Wang, L.; Yang, T.; Wu, Y.; Ding, Y.; Hu, A. *Polym. Chem.* **2019**, *10*, 2256–2262.
- (33) Jing, W.; Lu, Y.; Yang, G.; Wang, F.; He, L.; Liu, Y. Anal. Chim. Acta 2017, 985, 175–182.
- (34) Sener, G.; Uzun, L.; Denizli, A. ACS Appl. Mater. Interfaces 2014, 6, 18395–18400.
- (35) Huang, Y.; Cheng, P.; Tan, C. RSC Adv. 2019, 9, 27583-27587.
- (36) Wei, X.; Chen, Z.; Tan, L.; Lou, T.; Zhao, Y. Anal. Chem. 2017, 89, 556–559.
- (37) Tomita, S.; Ishihara, S.; Kurita, R. ACS Appl. Mater. Interfaces **2017**, 9, 22970–22976.
- (38) Xu, Q.; Zhang, Y.; Tang, B.; Zhang, C.-y. Anal. Chem. 2016, 88, 2051–2058.
- (39) Galpothdeniya, W. I. S.; Fronczek, F. R.; Cong, M.; Bhattarai, N.; Siraj, N.; Warner, I. M. J. Mater. Chem. B 2016, 4, 1414–1422.
- (40) Zhang, W.; Gao, N.; Cui, J.; Wang, C.; Wang, S.; Zhang, G.; Dong, X.; Zhang, D.; Li, G. Chem. Sci. 2017, 8, 6281–6289.
- (41) Shcherbakova, E. G.; Zhang, B.; Gozem, S.; Minami, T.; Zavalij, P. Y.; Pushina, M.; Isaacs, L. D.; Anzenbacher, P., Jr. *J. Am. Chem. Soc.* **2017**, *139*, 14954–14960.
- (42) Galpothdeniya, W. I. S.; Regmi, B. P.; McCarter, K. S.; de Rooy, S. L.; Siraj, N.; Warner, I. M. Anal. Chem. **2015**, 87, 4464–4471.

- (43) Minami, T.; Esipenko, N. A.; Akdeniz, A.; Zhang, B.; Isaacs, L.; Anzenbacher, P., Jr. J. Am. Chem. Soc. 2013, 135, 15238–15243.
- (44) Jurado, J. M.; Alcázar, A.; Muñiz-Valencia, R.; Ceballos-Magaña, S. G.; Raposo, F. *Talanta* **2017**, *172*, 221–229.
- (45) Araujo, P. J. Chromatogr., B: Anal. Technol. Biomed. Life Sci. 2009, 877, 2224–2234.
- (46) Murakami, S.; Yoshino, T. Talanta 1981, 28, 623-625.
- (47) Yoshino, T.; Murakami, S.; Ogura, K. J. Inorg. Nucl. Chem. 1979, 41, 1011-1013.
- (48) Lee, J.-S.; Lee, J. W.; Chang, Y.-T. J. Comb. Chem. 2007, 9, 926–928
- (49) Burdette, S. C. Eur. J. Inorg. Chem. 2015, 2015, 5728-5729.
- (50) Flynn, C. M., Jr. Chem. Rev. 1984, 84, 31-41.
- (51) Brereton, R. G. Chemometrics for pattern recognition; John Wiley & Sons: Chichester, U.K., 2009.